Modelling studies of enantioselective extraction of an amino acid derivative in slug flow capillary microreactors

Susanti, Susanti; Schuur, Boelo; Winkelman, Jozef; Heeres, Hero; Yue, Jun

Published in:
Chemical Engineering Journal

DOI:
10.1016/j.cej.2018.08.006

Document Version
Publisher's PDF, also known as Version of record

Publication date:
2018

Chemical Engineering Journal 354 (2018) 378–392

Contents lists available at ScienceDirect

Chemical Engineering Journal

journal homepage: www.elsevier.com/locate/cej

Modelling studies of enantioselective extraction of an amino acid derivative in slug flow capillary microreactors

Susanti[a], Boelo Schuur[b], Jozef G.M. Winkelman[a], Hero J. Heeres[a], Jun Yue[a,*]

[a] Department of Chemical Engineering, Engineering and Technology Institute Groningen, University of Groningen, 9747 AG Groningen, The Netherlands
[b] Sustainable Process Technology Group, Faculty of Science and Technology, University of Twente, 7500 AE Enschede, The Netherlands

HIGHLIGHTS

- Enantioselective extraction of 3,5-dinitrobenzoyl-*(R,S)*-leucine was modelled.
- Kinetic effects led to a higher *ee* of the *(S)*-enantiomer than the equilibrium *ee*.
- The complexation rate of the *(S)*-enantiomer with host was assumed instantaneous.
- The complexation rate of the *(R)*-enantiomer was possibly finite.
- The developed model allows to optimize multi-stage operation in microreactors.

ARTICLE INFO

Keywords:
Chiral separation
Liquid-liquid extraction
Microreactor
Slug flow
Mass transfer
Modelling

ABSTRACT

This work shows that enantioselective liquid–liquid extraction in microreactors is attractive for chiral separation. A precise control over the residence time in microreactors results in high enantiopurities and low host inventories. Mathematical modelling has been presented to describe the experimental results on the enantioselective extraction of an aqueous racemic amino acid derivative (3,5-dinitrobenzoyl-*(R,S)*-leucine) with a cinchona alkaloid chiral host in 1-octanol using a slug flow capillary microreactor (at an aqueous to organic flow ratio of 1:1). A good agreement between the model predictions and experimental results was obtained by taking the enhancement of the mass transfer rates due to the reactions in the aqueous and organic phases into account. An enantiomeric excess of the *(S)*-enantiomer higher than the equilibrium value was observed especially at shorter residence times due to kinetic effects. The observed phenomena could be explained by an instantaneous rate of the complexation of the *(S)*-enantiomer with the host and a finite rate of the complexation of the *(R)*-enantiomer. The developed model was used to determine guidelines for multi-stage operation in microreactors in order to increase yield and enantiopurity.

1. Introduction

In the last few decades, the demand for enantiopure compounds has increased rapidly [1–5]. For example, in pharmaceutical industries this is due to the often different biological activity of each enantiomer leading to different pharmacological activities and different pharmacokinetic or toxicity effects [1–4]. Racemic production followed by chiral separation is currently being used for the majority of the synthetic single enantiomer products [6,7].

Several methodologies for chiral separation have been reported and compiled in various reviews including crystallization [8–12], chromatography [1,8,13–16], capillary electrophoresis [8,14,15], membrane-based separations [8,17–21], and liquid–liquid extractions [6,8,22–43]. Crystallization and chromatographic methods seem to be the most advanced for chiral separations [8,12,14]. The main drawbacks of crystallization-based chiral separation methods are a limited flexibility and solid handling [8,35,37,41]. Chromatography-based methods have been demonstrated on small scale [8,14]. Although modifications allow for continuous operation on the preparative scale, this method is technically relatively complicated and suffers from high capital cost [6,8,16].

In enantioselective liquid–liquid extraction (ELLE), a solution of a racemic mixture is contacted with an immiscible solution containing a chiral host. The host complexates preferentially with one of the enantiomers. ELLE is an alternative when classical resolution using crystallization is not possible [44,45]. Several experimental and modelling

* Corresponding author.
E-mail address: yue.jun@rug.nl (J. Yue).

https://doi.org/10.1016/j.cej.2018.08.006
Received 30 April 2018; Received in revised form 1 August 2018; Accepted 2 August 2018
Available online 03 August 2018

Nomenclature

a	interfacial area per reactor volume, $m^2\,m^{-3}$
C	host or complexant
D	diffusivity, $m^2\,s^{-1}$
d_c	diameter of the microreactor, m
E	enhancement factor
f_C,f_R	$f_C = [C]_{org}/[C]_{org,I}$, $f_R = [R]_{org}/[R]_{org,I}$
g_R	$g_R = K_R \frac{D_{RC,org}}{D_{R,org}}[C]_{org,I}$
Ha_R	Hatta number for the (R)-enantiomer, $Ha_R = \sqrt{D_{R,org}k_{2,R}[C]_{org}}/k_{L,R,org}$
I	Ionic strength, mol m^{-3}
J	molar flux from the aqueous phase to the organic phase, $mol\,m^{-2}\,s^{-1}$
$k_{2,R}$	second-order forward reaction rate constant for the complexation of the (*R*)-enantiomer with the host, $m^3\,mol^{-1}\,s^{-1}$
K_a	acid dissociation constant, $mol\,m^{-3}$
k_L	liquid-phase mass transfer coefficient, $m\,s^{-1}$
K_{ov}	overall mass transfer coefficient, $m\,s^{-1}$
K_R	complexation constant for the *(R)*-enantiomer, $m^3\,mol^{-1}$
K_S	complexation constant for the *(S)*-enantiomer, $m^3\,mol^{-1}$
L_c	length of the microreactor, m
$L_{droplet}$	Length of droplet, m
L_{slug}	Length of liquid slug, m
m	Partition coefficient
Q	volumetric flow rate, $m^3\,s^{-1}$
R	*(R)*-enantiomer
RC	combined form of the *(R)*-enantiomer with the host
RSD	relative standard deviation
S	*(S)*-enantiomer
SC	combined form of the *(S)*-enantiomer with the host
SSR	sum of the squares of residuals
T	temperature, °C
V	volume, m^3
x	distance from the interface, m
Y	yield

Greek symbols

γ	activity coefficient
δ	film thickness according to the film model, m
μ	viscosity, Pa s
ρ	density, $kg\,m^{-3}$
σ	surface tension, $N\,m^{-1}$
τ	residence time, s
ϕ_R	$\phi_R = \delta_{org}\sqrt{\frac{k_{2,R}[C]_{org,I}}{D_{R,org}}\frac{g_R+1}{g_R}}$
φ	association factor, see Eq. (31)
$\Re$	production rate of a species, $mol\,m^{-3}\,s^{-1}$

Subscript

∞	instantaneous reaction
A	solute or species A (S, S^-, R, R^-, C, SC, RC)
all	all or total
aq	aqueous
B	solvent B
bulk	in the bulk of a phase
C	host or complexant
chem	chemical
I	at the interface between two phases
in	at inlet
org	organic
out	at outlet
phys	physical
R	*(R)*-enantiomer
RC	combined form of the *(R)*-enantiomer with the host
S	*(S)*-enantiomer
SC	combined form of the *(S)*-enantiomer with the host
x	ion x

Abbreviation

1,2-DCE	1,2-dichloroethane
CA	cinchona alkaloid
CCCS	continuous centrifugal contactor separator
DNB	3,5-dinitrobenzoyl
ee	enantiomeric excess
ELLE	enantioselective liquid–liquid extraction
HPLC	high-performance liquid chromatography
PTFE	polytetrafluoroethylene

studies on ELLE for the separation of a racemic mixture to obtain an enantiopure compound have been reported [6,22–43,46–54]. Advantages of ELLE include the ease of scale up and the possibility to use one host family for the separation of multiple racemates [8,35,43].

The proof of concept for ELLE in a continuous centrifugal contactor separator (CCCS) has been reported [32,33,46–48]. For example, ELLE of 3,5-dinitrobenzoyl-*(R,S)*-leucine (DNB-*(R,S)*-Leu) with a cinchona alkaloid (CA) host in 1,2-dichloroethane (1,2-DCE) has been demonstrated in a single CCCS. An *(S)*-enantiomer excess (ee_{org}) of 34% and a yield of 61% were obtained [32]. With six CCCS devices in series, operated countercurrently, up to 98% *ee* was obtained [33]. However, a large host inventory was present due to the high hold-up of the organic phase in the CCCS devices, indicating a significant cost increase.

Alternatives to a CCCS for continuous ELLE have been reported with the use of intensified columns and microreactors [25,26,44]. Kockmann and co-workers [25,26] have reported the use of intensified columns for similar systems (ELLE of DNB-*(R,S)*-Leu with a CA host). The process involved countercurrent operation with stirring and pulsation, resulting in a large number of stages and a good separation with an *ee* of up to 98.6% and 85.8% for the *(R)*- and *(S)*-enantiomers, respectively [26]. Microreactors operated under slug flow are another alternative for ELLE, with advantages including a precise process control, an enhanced extraction efficiency, a reduced reactor volume, a low host and solvent inventory, and easy scaling-up [55–63]. Such slug flow microreactors offer a superior control over the temperature and residence time [64,65]. Both are critical for obtaining a high operational selectivity in chiral separation [66]. The mass transfer and extraction rates are enhanced by internal circulation in the droplets and liquid slugs [67]. Microreactors for ELLE have simple setups without moving parts and are relatively easy to scale up to pharmaceutical production scales [60,68].

Recently, we have investigated ELLE in capillary microreactors under slug flow operation for the enantioselective extraction of an aqueous solution of DNB-*(R,S)*-Leu (Fig. 1) with a cinchona alkaloid host that was applied in organic solvents including 1,2-DCE and 1-octanol [44]. The experiments showed that the concentration of the enantiomers at the microreactor outlet turned out to be a function of the residence time for a given aqueous to organic flow ratio and

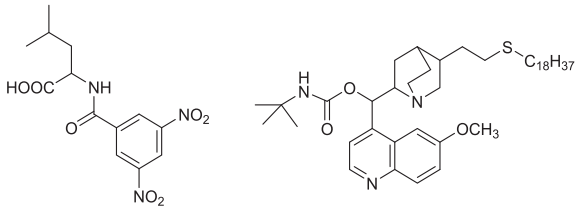

DNB-*(R,S)*-Leu **CA**

Fig. 1. DNB-*(R,S)*-Leu and cinchona alkaloid (CA) considered in this work.

enantiomer/host intake. Interestingly, when using 1-octanol as the solvent, the *(S)*-enantiomer excess in the organic phase was higher at short residence times than the *ee* at equilibrium. This finding indicates that non-equilibrium ELLE operation in microreactors may have high potential for future application. A detailed mass transfer and extraction analysis to identify the factors responsible for the above findings is thus the main purpose of this work.

2. Experimental method

2.1. Materials

The amino acid derivative, 3,5-dinitrobenzoyl-*(R,S)*-leucine (DNB-*(R,S)*-Leu), was obtained from DSM. The host cinchona alkaloid (CA; Fig. 1) was synthesized according to the literature procedure [44,69]. The organic diluent, viz. 1-octanol (99.8%) was purchased from Sigma-Aldrich. Disodium hydrogen phosphate (≥99.5%) and potassium dihydrogen phosphate (≥99.5%) for use as the aqueous buffer system were obtained from Merck. All experiments were performed with Milli-Q water.

2.2. ELLE in capillary microreactors

The extraction procedure and experimental apparatus have been described in detail previously [44]. Here a brief overview is provided, with the flow and ELLE schematics shown in Fig. 2. The aqueous phase inlet consisted of 1 mM DNB-*(R,S)*-leu in 0.1 M phosphate buffer (pH 6.58) and organic phase inlet 1 mM CA in 1-octanol. Extraction experiments were operated in the slug flow regime using capillary microreactors made of polytetrafluoroethylene (PTFE) tubing with an inner diameter of 0.8 mm, under conditions as shown in Table 1. After extraction in the microreactor, the immiscible liquids were separated at the end of the microreactor using a Y-splitter consisting of a PTFE exit and a glass exit. Phase separation is based on the preferential wettability (i.e., the aqueous phase prefers glass, the organic phase PTFE). The compositions of the aqueous phase at the microreactor inlet and outlet were analyzed via HPLC.

As can be seen in Table 1, the extraction was carried out in the microreactor of different lengths at an aqueous to organic flow ratio of 1:1. The residence time (τ) was between 22 and 905 s, which is defined as

$$\tau = \frac{V_c}{Q_{aq} + Q_{org}} = \frac{\frac{\pi}{4} d_c^2 L_c}{Q_{aq} + Q_{org}} \quad (1)$$

where V_c, d_c and L_c are the volume, inner diameter and length of the capillary microreactor, respectively. Q_{aq} and Q_{org} denote the volumetric flow rates of the aqueous and organic phases, respectively.

Table 1
Experimental conditions for ELLE of DNB-(*R*,*S*)-Leu in a capillary microreactor [44].

Operating parameter	Value	Ranges
Temperature (°C)	Ca. 23	
Buffer concentration (M)	0.1	
Buffer pH	6.58	
DNB-*(R,S)*-Leu concentration (mM)	1	
CA host concentration (mM)	1	
Capillary inner diameter (mm)	0.8	
Capillary length (cm)		12.5–250
Q_{aq}, Q_{org} [mL/h]		2.5–7.5
Q_{aq}/Q_{org}	1	

2.3. Determination of ELLE equilibrium constants in batch reactors

Here, batch experiments with 1-octanol as solvent are described. The experiments were carried out in 20 mL glass flasks. A series of 10 mL unbuffered aqueous DNB-*(R,S)*-Leu solutions with a concentration in a range of (0.5–3.2) × 10^{-4} mol/L were mixed with 1 mL 1-octanol to determine the physical partitioning over the phases in the absence of CA. Stirring was done with a Teflon bar for 14 h. Afterwards, both phases were allowed to settle for one hour and separated. The pH of the aqueous phase was measured and its composition was analyzed by HPLC. The enantiomer concentration in the organic phase was calculated according to the mass balance.

The complexation constants for the reactions between each enantiomer and CA were determined using reactive extraction. 1 mL buffered (pH 6.58) racemic aqueous DNB-*(R,S)*-leu solution (1 mM) and 1 mL of host solution (1 mM) were mixed in 20 mL glass flasks under stirring using a Teflon bar for 14 h. After equilibrium and settling, both phases were separated. The enantiomer concentration in the aqueous phase was analyzed by HPLC. The organic phase concentration was calculated according to the mass balance.

2.4. Analytical procedure

Concentrations of the enantiomers in the aqueous phase were measured using HPLC (Shimadzu SIL-20A) equipped with a chiral column (Astec/Chirobiotic T). The eluent was a 3:1 (v/v) mixture of acetonitrile and methanol with 0.25 vol.% triethylamine and 0.25 vol.% acetic acid. The pH of the aqueous phase was measured using an InoLab pH 730 pH-meter equipped with a SenTix 81 probe (WTW, Germany).

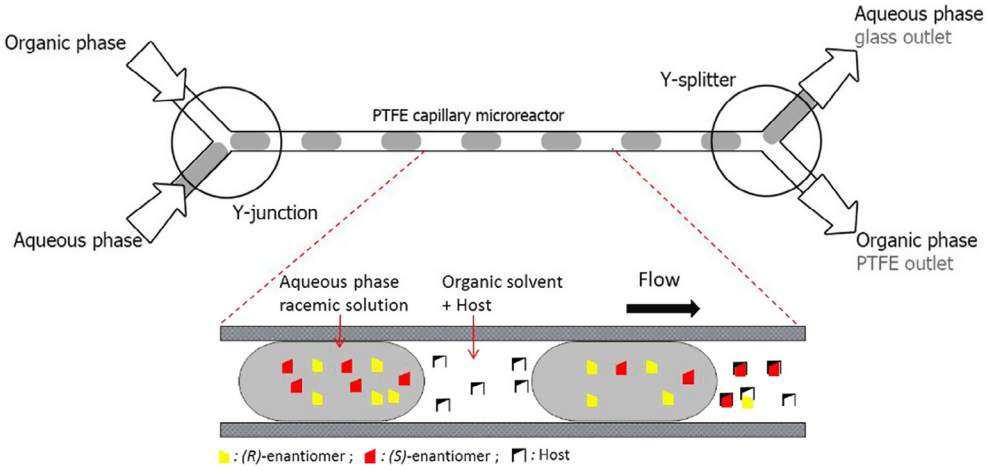

Fig. 2. Scheme of ELLE under slug flow operation in a microreactor (condition for a hydrophobic microreactor wall).

3. Model development

The scheme of the extraction mechanism is similar to the model used and validated by Schuur et al. [35,70], see Fig. 3. DNB-*(R,S)*-Leu is a weak acid [70], so it exists in the aqueous phase in the neutral and dissociated forms. Only the neutral form is transported to the organic phase and can combine with the host.

The component balance of the *(S)*-enantiomer in the aqueous phase when flowing in the microreactor reads

$$Q_{aq}\frac{d[S]_{aq,all}}{dV_c} = -J_{S,aq}a \;\; (V_c = 0: \;\; [S]_{aq,all} = [S]^{in}_{aq,all}) \tag{2}$$

where $[S]_{aq,all} = [S]_{aq} + [S^-]_{aq}$ and J_S denotes the molar flux of the *(S)*-enantiomer from the aqueous phase to the organic phase. Similarly, for the *(R)*-enantiomer we have

$$Q_{aq}\frac{d[R]_{aq,all}}{dV_c} = -J_{R,aq}a \;\; (V_c = 0: \;\; [R]_{aq,all} = [R]^{in}_{aq,all}) \tag{3}$$

where $[R]_{aq,all} = [R]_{aq} + [R^-]_{aq}$. The corresponding balances for the organic phase read

$$Q_{org}\frac{d[S]_{org,all}}{dV_c} = J_{S,org}a \;\; (V_c = 0: \;\; [S]_{org,all} = 0) \tag{4}$$

$$Q_{org}\frac{d[R]_{org,all}}{dV_c} = J_{R,org}a \;\; (V_c = 0: \;\; [R]_{org,all} = 0) \tag{5}$$

where $[S]_{org,all} = [S]_{org} + [SC]_{org}$ and $[R]_{org,all} = [R]_{org} + [RC]_{org}$.

3.1. Calculation of the molar fluxes

In mass transfer applications, the fluxes between different phases are usually calculated using one of two widely used models: the film model or the penetration model [71]. The fluxes are obtained from solving a set of equations that describe the combined effects of diffusive transport and reactions in a particular phase near the interface. Applying the film model, we have for the aqueous phase

$$\begin{aligned} D_{A,aq}\frac{\partial^2[A]_{aq}}{\partial x^2} &= -\Re_{A,aq} \quad (A = S, S^-, R, R^-) \\ x = 0: \;\; [A]_{aq} &= [A]_{aq,I} \\ x = \delta: \;\; [A]_{aq} &= [A]_{aq,bulk} \end{aligned} \tag{6}$$

where $[A]$ denotes the concentration of species A in the film in the aqueous phase, $\Re_{A,aq}$ denotes its local production rate, x is the distance from the interface and δ is the so-called film thickness of the film model. Analogously, for the organic phase a set of equations, one for each component (i.e., S, R, C, SC or RC; Fig. 3), can be written. Both sets can then be solved simultaneously for the gradients at the interface that allow for the calculation of the interfacial fluxes. The equations for the two phases are coupled at the interface by the solubility condition

$$m = \frac{[S]_{org,I}}{[S]_{aq,I}} = \frac{[R]_{org,I}}{[R]_{aq,I}} \tag{7}$$

The partition coefficient (m) was determined from physical extraction experiments in the absence of a pH buffer in batch reactors, using DNB-(*R,S*)-Leu solutions with a concentration in a range of (0.5–3.2) × 10^{-4} M (Section 2.3). m was found to be a constant of 26.73 according to Eq. (7). The constant value of m is reasonable and also applicable in the current microreactor study that dealt with a diluted enantiomer concentration in both the organic and aqueous phases. For example, ELLE experiments in microreactors (and the subsequent modelling thereof) were performed for an inlet aqueous concentration of DNB-*(R,S)*-Leu at 1 mM in the presence of a buffer (pH 6.58). Under such pH conditions (≫pK_a), each enantiomer was present in the aqueous phase predominantly in the dissociated form (Fig. 3) and thus the concentration of each enantiomer in the neutral form therein was at a very low level (ca. on the order of 10^{-7} M).

The solution of coupled sets of nonlinear differential equations in the form of Eq. (6) can be circumvented by using the concept of chemical enhancement factors. Then, the mass transfer rates can be obtained from the physical fluxes, i.e. without reaction, augmented by the enhancement factors. The partial fluxes can be written in the following form for the aqueous phase

$$J_{S,aq} = k_{L,S,aq}E_{S,aq}([S]_{aq,bulk} - [S]_{aq,I}) \tag{8}$$

$$J_{R,aq} = k_{L,R,aq}E_{R,aq}([R]_{aq,bulk} - [R]_{aq,I}) \tag{9}$$

and for the organic phase

$$J_{S,org} = k_{L,S,org}E_{S,org}([S]_{org,I} - [S]_{org,bulk}) \tag{10}$$

$$J_{R,org} = k_{L,R,org}E_{R,org}([R]_{org,I} - [R]_{org,bulk}) \tag{11}$$

The interface concentrations of Eqs. (8)–(11) are coupled by the solubility according to Eq. (7). Due to mass conservation, $J_{S,aq} = J_{S,org}$, and hence the subscripts aq and org in J_S and J_R are not required. Thus, the set of Eqs. (7)–(11) may be rewritten as

$$J_S = K_{ov,S}([S]_{aq} - \frac{[S]_{org}}{m}) \tag{12}$$

$$J_R = K_{ov,R}([R]_{aq} - \frac{[R]_{org}}{m}) \tag{13}$$

where the overall mass transfer coefficients of the *(S)*- and *(R)*- enantiomers follow from

$$(K_{ov,S})^{-1} = (k_{L,S,aq}E_{S,aq})^{-1} + (mk_{L,S,org}E_{S,org})^{-1} \tag{14}$$

$$(K_{ov,R})^{-1} = (k_{L,R,aq}E_{R,aq})^{-1} + (mk_{L,R,org}E_{R,org})^{-1} \tag{15}$$

3.2. Bulk phase concentrations

In the aqueous phase, the ionization reactions (see Fig. 3) are assumed to be very fast and to be always at equilibrium [72]. Then, the aqueous liquid bulk phase concentrations follow from the dissociation equilibria

$$K_a = \frac{\gamma_{S^-}\gamma_{H^+}}{\gamma_S}\frac{[S^-]_{aq}[H^+]_{aq}}{[S]_{aq}} = \frac{\gamma_{R^-}\gamma_{H^+}}{\gamma_R}\frac{[R^-]_{aq}[H^+]_{aq}}{[R]_{aq}} \tag{16}$$

and the component balances for the enantiomers:

$$[S]_{aq,all} = [S]_{aq} + [S^-]_{aq} \tag{17}$$

$$[R]_{aq,all} = [R]_{aq} + [R^-]_{aq} \tag{18}$$

In the organic phase, the reaction is also assumed to be fast enough that the complex formation is always at equilibrium:

$$K_S = \frac{[SC]_{org}}{[C]_{org}[S]_{org}} \tag{19}$$

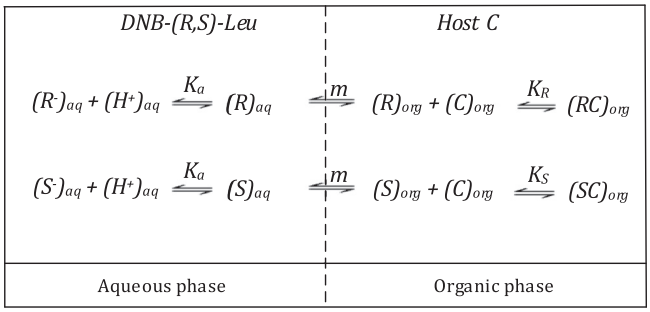

Fig. 3. ELLE mechanism of DNB-*(R,S)*-Leu with host C. Adapted from [70], Copyright (2008), with permission from American Chemical Society.

$$K_R = \frac{[RC]_{org}}{[C]_{org}[R]_{org}} \tag{20}$$

The organic phase bulk concentrations can be calculated from Eqs. (19) and (20) together with the component balance of the host

$$[C]_{org,all} = [C]_{org} + [RC]_{org} + [SC]_{org} \tag{21}$$

Here $[C]_{org,all} = [C]^{in}_{org,all}$ (i.e., no dissolution of the host and its complex forms in the aqueous phase; see Fig. 3).

3.3. Physico-chemical parameters

3.3.1. Interfacial area

The interfacial area (a) in slug flow was calculated [67], based on our experimental measurements on the droplet lengths (3.57 ± 0.15 mm) and slug lengths (3.53 ± 0.04 mm) using

$$a = \frac{4L_{droplet}}{d_c(L_{droplet} + L_{slug})} \tag{22}$$

Given the fixed 1:1 aqueous to organic flow ratio used, a was found to be almost constant (ca. 2488 ± 46 m^2/m^3).

3.3.2. Overall mass transfer coefficient

In our previous work [67], the overall physical mass transfer coefficient without reaction for the investigated microreactor under slug flow operation has been developed based on the penetration theory and additional contribution of internal circulation as

$$K_{ov,S,phys} = 2.6((2\sqrt{D_{S,aq}/\pi\tau})^{-1} + (2m\sqrt{D_{S,org}/\pi\tau})^{-1})^{-1} \tag{23}$$

Eq. (23) is for the case of the *(S)*-enantiomer (and similarly for the *(R)*-enantiomer). To allow for mass transfer enhancement due to the chemical reactions in both phases, the enhancement factors have to be incorporated. Thus, the overall mass transfer coefficient with chemical reactions is obtained for the case of the *(S)*-enantiomer as

$$K_{ov,S,chem} = 2.6((2E_{S,aq}\sqrt{D_{S,aq}/\pi\tau})^{-1} + (2mE_{S,org}\sqrt{D_{S,org}/\pi\tau})^{-1})^{-1} \tag{24}$$

Eqs. (23) and (24) are applicable for the current chiral extraction system, given 1:1 aqueous to organic flow ratio, Fourier number typically < 0.1, and the fact that the extraction performance at a constant temperature indeed turned out to be just a function of the residence time (i.e., independent of the flow rate or microreactor length; cf. Appendix A).

3.3.3. Enhancement factor

Enhancement factors according to the film model can be calculated by solving the simultaneous sets of differential equations (Eq. (6)) for the aqueous phase or similar ones for the organic phase. Fortunately, fairly accurate estimation methods are available to calculate the enhancement factors. Generally, these methods obtain an approximate analytical solution by applying a suitable linearization of the differential equations.

Regarding the complexation of each enantiomer with the host in the organic phase, using the results of Onda et al. [73] rewritten in our notation gives for the *(R)*-enantiomer

$$E_{R,org} = \frac{1 + g_R[1 + \frac{1-f_C}{1-f_R}f_R(1-\mathrm{sech}\,\phi_R)]}{1 + g_R\frac{\tanh\phi_R}{\phi_R}} \tag{25}$$

where the equilibrium constant is contained in the parameter g_R and the second-order forward reaction rate constant ($k_{2,R}$) in the parameter ϕ_R. The parameters are defined in the Nomenclature section. Note that here the complexation is assumed first order with respect to the enantiomer and the host, respectively.

In the limiting case where the reaction rate in the film is much faster than the diffusion rate, Eq. (25) simplifies to the so-called enhancement factor for an instantaneous reaction [74]:

$$E_{R,org,\infty} = 1 + \frac{D_{C,org}}{D_{R,org}}\frac{[C]_{org}}{[R]_{org,I} + \frac{D_{C,org}}{K_R D_{RC,org}}} \tag{26}$$

Similarly, the enhancement factor for an instantaneous reaction in the case of the *(S)*-enantiomer reads

$$E_{S,org,\infty} = 1 + \frac{D_{C,org}}{D_{S,org}}\frac{[C]_{org}}{[S]_{org,I} + \frac{D_{C,org}}{K_S D_{SC,org}}} \tag{27}$$

The dissociation of each enantiomer in the aqueous phase is assumed in equilibrium everywhere in the aqueous phase. Accordingly, $E_{S,aq} = E_{R,aq} = E_{aq,\infty}$.

$$E_{aq,\infty} = 1 + \frac{D_{S^-,aq}\gamma_S K_a}{D_{S,aq}\gamma_{H^+}\gamma_{S^-}[H^+]_{aq}} = 1 + \frac{D_{R^-,aq}\gamma_R K_a}{D_{R,aq}\gamma_{H^+}\gamma_{R^-}[H^+]_{aq}} \tag{28}$$

$E_{aq,\infty}$ is a constant under the present conditions (pH 6.58) and denotes the instantaneous enhancement factor for the dissociation of the *(S)*- or *(R)*-enantiomer in the aqueous phase (see Appendix B for details). Here, the diffusivities of each enantiomer in its neutral and dissociated forms are assumed equal for a first approximation (i.e., $D_{S,aq} \approx D_{S^-,aq}$ and $D_{R,aq} \approx D_{R^-,aq}$).

3.3.4. Activity coefficient

The activity coefficients (γ) of the ionic species in the aqueous solution were obtained from the Debye-Hückel law [75].

$$\log(\gamma_x) = \frac{-pz_x^2 I^{1/2}}{1 + qI^{1/2}} \tag{29}$$

where z_x is the charge number of the ion species x. The values of the constants p and q for the aqueous sodium chloride solutions at 25°C were taken here as an approximation (i.e., $p = 0.5115$ and $q = 1.316$) [75]. The ionic strength (I) is calculated according to

$$I = \frac{1}{2}\sum_x z_x^2 C_x \tag{30}$$

where C_x denotes the molarity (mol/L) of the ionic species x. Since the concentrations of the enantiomers in the neutral forms were very low in this study (ca. on the order of 10^{-7} M), their activity coefficients are assumed to be 1.

3.3.5. Physical properties of the system

The physical properties of the solvent and chemicals used are shown in Tables 2 and 3. The diffusivities of chemicals (in water and 1-octanol) were estimated based on the Wilke-Chang equation [76]

$$D_{A,B} = \frac{7.4 \times 10^{-8}(\varphi_B M_B)^{1/2}T}{\mu_B v_A^{0.6}} \tag{31}$$

Here $D_{A,B}$ represents the diffusivity of solute A in solvent B. The solvent viscosity (μ_B) is in cP, the solute molar volume at the normal boiling point (v_A) is in cm^3/mol and φ_B represents the solvent association (being 2.6 for water, 1.9 for methanol, 1.5 for ethanol and 1 for unassociated solvents) [76]. Since the diffusivity approximation using the Wilke-Chang equation is applicable for solvents like water, low alcohol (e.g., methanol, ethanol) and unassociated ones, the enantiomer and host diffusivities in 1-octanol were approximated following the Stokes-Einstein equation (Eq. (32)), using the corresponding diffusivities in water

Table 2
Physical properties of the solvents used (T = 25°C) [78].

Liquid	Density [kg/m^3]	Viscosity [Pa s]	Surface tension with water [N/m]
Water	998	8.9×10^{-4}	–
1-octanol	822	7.3×10^{-3}	8.19×10^{-3}

Table 3
Diffusivity of solute in the solvent (T = 25 °C).

Solvent	Diffusivity [m^2/s]	
	DNB-*(R,S)*-Leu	CA
Water	4.9×10^{-10} [(a)]	–
1-octanol	5.98×10^{-11} [(b)]	4.84×10^{-11} [(b)]

[(a)] calculated by Eq. (31); [(b)] Calculated by Eq. (32).

and 1,2-DCE as a reference, respectively [77].

$$\frac{D_{A,B}\mu_B}{T} = \text{constant} \tag{32}$$

The diffusivities of host (C) and its combined form (SC or RC) are assumed to be equal for a first approximation, given the much larger molar volume of host than that of the enantiomer.

3.4. Numerical solution method

The concentrations of the enantiomers in the microreactor were obtained by numerically solving the reactor equations (Eqs. (2)–(5)) in an outer loop. A stepwise approach was employed where the microreactor was divided into n equally-spaced segments (see Fig. 4). At sufficiently large values of n, the concentrations can be taken constant within each segment k (k = 1, 2, …, n), given negligible amount of extraction therein. From the concentrations in the two phases, the mass transfer rates of the components were calculated using the methods of Sections 3.1–3.3. The mass transfer rates were obtained iteratively in an inner loop. They were used to update the host and enantiomer concentrations at the outlet of the segment to account for the extraction within the segment in order to fulfil the mass balance. The modelling then proceeded to the next segment. This numeric approximation converges at sufficiently large n values (see Appendix C for more detailed discussion). The mathematical formulation was translated to computer codes and solved using Matlab software (version R2016a, The Mathworks Inc.).

4. Results and discussion

4.1. Equilibrium extraction

The equilibrium constants for the complexation reaction between DNB-*(R,S)*-Leu and CA in the 1-octanol system are shown in Table 4. The value of K_S is higher than K_R, indicating that the host CA preferentially complexates with the *(S)*-enantiomer over the *(R)*-enantiomer similar to the 1,2-DCE system as reported by Schuur et al. [70]. Also the intrinsic selectivity, defined as K_S/K_R, is comparable in 1-octanol and 1,2-DCE, with values of 3.24 and 3.43, respectively [70]. With this selectivity nine equilibrium stages are required to obtain at least 99% *ee* in both phases under total reflux conditions according to the Fenske equation [70].

4.2. Modelling results of ELLE in microreactors

4.2.1. Model I: instantaneous complexation rate for both the (S)- and (R)-enantiomers

In a first approach the complexation reactions were assumed to proceed in the instantaneous reaction regime for both enantiomers (model I). The system was thus modelled using the method described in Section 3.4, where the enhancement factors of the (*R*)- and (*S*)-enantiomers in the organic phase were obtained from Eqs. (26) and (27), respectively. The relative standard deviation (RSD) between the modelled and experimental values was taken as the indicator for the quality of the model performance, which is calculated by

$$\text{RSD} = \sqrt{\frac{1}{N-1}\sum_{i=1}^{N}\left(\frac{y_{\text{model},i}-y_{\text{exp},i}}{y_{\text{exp},i}}\right)^2} \times 100\% \tag{33}$$

where N is the number of data points. $y_{\text{model},i}$ and $y_{\text{exp},i}$ denote the modelled and experimental values of the parameter (in this case being the enantiomer concentration or the enantiomeric excess) at a specific data point i, respectively. With model I, the aqueous phase exit concentration of the *(S)*-enantiomer was modelled with an RSD of 10.2%. The fit is better at relatively short residence times and a slight larger deviation exists at relatively large residence times approaching equilibrium (Fig. 5). The corresponding concentrations of the *(R)*-enantiomer were predicted better, with an RSD of 4.6%.

An important parameter in enantiomeric separation is the enantiomeric excess (*ee*), defined for the current system as

$$ee_{aq} = \frac{[R]^{out}_{aq,all} - [S]^{out}_{aq,all}}{[R]^{out}_{aq,all} + [S]^{out}_{aq,all}} \times 100\% \tag{34}$$

$$ee_{org} = \frac{[S]^{out}_{org,all} - [R]^{out}_{org,all}}{[S]^{out}_{org,all} + [R]^{out}_{org,all}} \times 100\% \tag{35}$$

The observed and modelled *ee* data are shown in Fig. 6. The modelled values show large deviations from the experimental data. Also the predicted ee_{org} shows a faulty qualitative behavior with a small initial increase whereas a considerable initial decrease was observed experimentally. A detailed analysis of the results showed that the deviations of the *ee* are mainly due to an underestimation in the modelled $[R]^{out}_{aq,all}$ values at relatively short residence times (e.g., ca. at τ < 90 s) and an overestimation of the modelled $[S]^{out}_{aq,all}$ values at relatively large residence times (see Fig. 5). In other words, a good modelling of the *ee* is highly sensitive to the prediction accuracy of the enantiomer concentration.

4.2.2. Model II: instantaneous complexation rate for the (S)-enantiomer and finite complexation rate for the (R)-enantiomer

The observed deviations with model I, both in the exit concentrations and the *ee* values, suggest that the complexation rate of the *(R)*-enantiomer is not fast enough to be taken as instantaneous. Therefore in model II, the complexation of the *(R)*-enantiomer is taken to proceed with a finite rate. The complexation of the *(S)*-enantiomer is still assumed to proceed instantaneously. In more detail, the system was modelled using the method described in Section 3.4. The enhancement factor of the (*S*)-enantiomer in the organic phase was obtained from Eq. (27), and that of the (*R*)-enantiomer was obtained from Eq. (25) based on an assumed value of the second-order forward reaction rate constant ($k_{2,R}$) for its complexation with the host. In the modelling, the optimized value of $k_{2,R}$ was determined, at which the deviation between the model prediction and the measured ee_{org} value (expressed as the sum of the squares of residuals (SSR); see definition in Eq. (36)) reached its minimum.

$$\text{SSR} = \sum_{i=1}^{N}(y_{\text{model},i}-y_{\text{exp},i})^2 \tag{36}$$

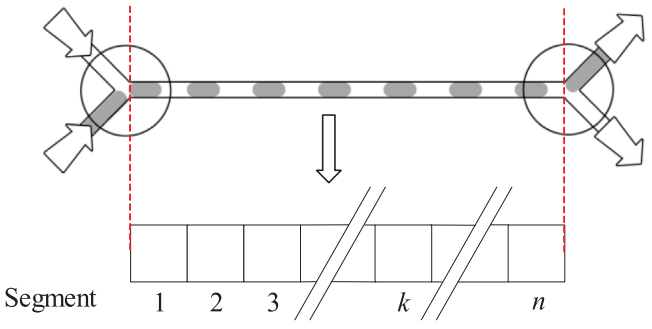

Fig. 4. Equally-spaced segments of the microreactor used in the modelling.

Table 4
Equilibrium constants involved in ELLE of DNB-*(R,S)*-Leu with CA in 1-octanol at room temperature.

Parameter	Value	Dimension
K_a	1.92×10^{-4} (a)	mol/L
Partition coefficient (m)	26.73 (b)	–
K_S	1.21×10^{5} (b)	L/mol
K_R	3.73×10^{4} (b)	L/mol

(a) Literature [70]; (b) Measured in the current work.

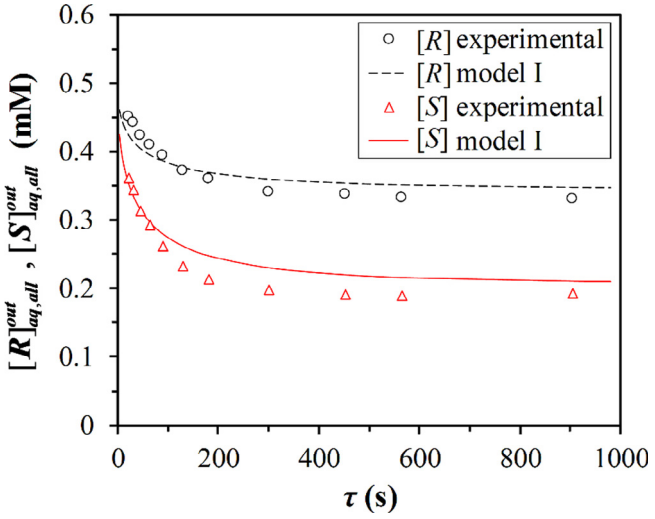

Fig. 5. Aqueous phase exit concentrations versus the residence time in the microreactor according to the experiments and model I. Error bar is not shown since the standard deviation between the measured data from at least two repetitive experimental runs is too small to be visible here.

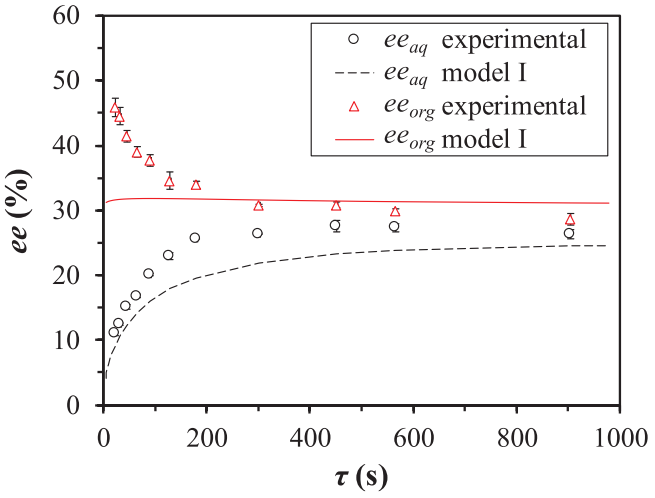

Fig. 6. Enantiomeric excess values at the microreactor outlet as a function of the residence time according to the experiments and model I. Error bar indicates the standard deviation measured from at least two repetitive experimental runs.

The optimized value of $k_{2,R}$ with a 95% confidence interval was found as $(5 \pm 1.1) \times 10^5$ L/(mol·s). The 95% confidence interval was estimated based on the following equation [79]

$$SSR_{95\%} = SSR_{min}\left(1 + \frac{1}{N-1}F(1, N-1, 0.95)\right) \quad (37)$$

where SSR_{min} and $SSR_{95\%}$ are the minimum value of SSR related to the ee_{org} and the value of SSR at a 95% confidence level, respectively. The

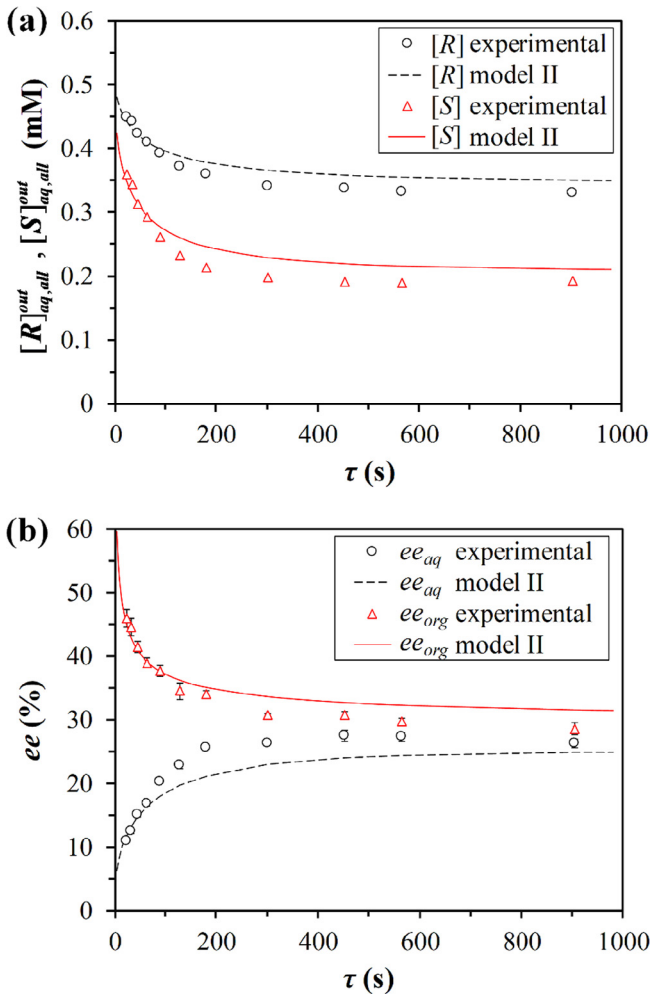

Fig. 7. Comparison of the experimental values with the predictions of model II versus the residence time. (a): the aqueous phase exit concentrations. (b): the enantiomeric excess (*ee*).

function F represents the F-distribution. With the estimated $SSR_{95\%}$ from Eq. (37), the corresponding lower and upper limits of $k_{2,R}$ in the confidence interval were subsequently obtained from the modelling.

With this model II, the aqueous phase exit concentrations as well as the ee_{org} and ee_{aq} were modelled satisfactory, see Fig. 7a and 7b, respectively. Importantly, the ee_{org} values now have a correct qualitative and quantitative behavior as a function of the residence time. The relative standard deviations of the predicted values as compared to the measured data were 5.7% and 10.3% for the ee_{org} and ee_{aq}, respectively (Table 5). The improved performance of model II can be attributed mainly to a more accurate representation of the exit concentration of the *(R)*-enantiomer, especially at relatively short residence times (Fig. 7a).

The optimized value of $k_{2,R}$ at 5×10^5 L/(mol·s) implies that the rate of complexation of the *(R)*-enantiomer is intrinsically fast. This is

Table 5
Comparison of the prediction performance of models I and II.

Model	RSD in the prediction of the aqueous phase exit concentration		RSD in the prediction of the enantiomeric excess	
	$[S]^{out}_{aq,all}$	$[R]^{out}_{aq,all}$	ee_{org}	ee_{aq}
I	10.2%	4.6%	18%	18.1%
II	9.6%	4.2%	5.7%	10.3%

supported by the results of separate observations with batch reactors (not shown here) where equilibrium was reached within 1 min after mixing of equal amounts of the aqueous and organic phases. The reaction regime of the complexation of the *(R)*-enantiomer in relation to the mass transfer rate in the organic phase can be identified by considering the Hatta number (Ha_R) and the enhancement factor ($E_{R,org}$). Both numbers are plotted versus the residence time in Fig. 8 according to model II. Generally, the rate of the reaction is considered instantaneous compared to the rate of mass transfer if $Ha_R \gg E_{R,org}$ [73]. From Fig. 8, it is clear that this criterion is satisfied only at relatively long residence times (e.g., at $\tau > 50$ s). Especially at short residence times, the reaction regime for the complexation of the *(R)*-enantiomer was in either the slow or fast complexation regime [80], but not in the instantaneous regime.

The experimental observations and the results of model II show that at short residence times, a high ee_{org} can be achieved. Importantly, the ee_{org} values found here are much higher than the values at equilibrium conditions (i.e., obtained at sufficiently long residence times). These results could be obtained with the microreactor because it allows for slug flow operation with short residence times and an intrinsically narrow residence time distribution [81]. With short residence times, the extraction rate of the *(R)*-enantiomer was determined by both the physical mass transfer rate as well as the complexation rate. At the same time the extraction rate of the *(S)*-enantiomer was completely mass transfer limited (given the instantaneous complexation rate assumed). Therefore, it is the kinetic effect of the *(R)*-enantiomer complex formation that primarily caused the high ee_{org} at short residence times. In other words, at such short residence times the intrinsic complexation rate of each enantiomer, when compared with the physical mass transfer rate, showed a large difference, which resulted in a more favorable enrichment of the *(S)*-enantiomer. Thus, a higher ee_{org} values than the equilibrium ones were obtained. The results obtained here with model II further suggest that such chiral separations can be realized in a highly controllable and predictive way in slug flow microreactors.

4.3. Process simulation for multi-stage ELLE operation

Using the current microreactor system, a high ee_{org} can be achieved by performing chiral extraction at short residence times. However, the yield of the *(S)*-enantiomer is very low then [44]. To improve the yield, a multi-stage ELLE operation is suggested. Here two options for multi-stage operation are modelled and discussed.

The first option is a cross flow configuration where the aqueous stream continuously flows from one stage to the next and fresh organic feed is supplied at each stage (Fig. 9). The flow rate ratios between the organic and aqueous phases are kept the same in all stages (i.e., at 1:1). The exit concentrations for each stage were obtained using model II. The overall ee_{org} and the overall yield of the *(S)*-enantiomer were obtained from Eqs. (35) and (38), respectively.

$$Y_S = \frac{[S]^{in}_{all,aq} - [S]^{out}_{all,aq}}{[S]^{in}_{all,aq}} \times 100\% \quad (38)$$

The performance of cross flow extraction was assessed by varying the total number of stages from 1 to 5 and using a residence time per stage of 4, 10, 22.6 or 45.2 s. At shorter residence times, it is possible to obtain a higher overall ee_{org} than the equilibrium value, see Fig. 10. Smaller residence times per stage yield higher ee_{org} values. The overall yield of the *(S)*-enantiomer increases with an increase of the total number of stages due to additional extraction per stage. The overall ee_{org} decreases with an increasing number of stages since, from the second stage onwards, the aqueous phase is more and more enriched with the *(R)*-enantiomer. Under such circumstances, the extraction of the *(R)*-enantiomer is increasingly important compared with the extraction of the *(S)*-enantiomer. Noteworthy, such decrease in the overall ee_{org} is not very pronounced at the shortest residence time modelled (i.e., $\tau = 4$ s per stage). Whereas for $\tau = 45.2$ s or 22.6 s per stage, the extraction should be stopped at stage 3 or 4, respectively, since the organic effluent at the next stage is already slightly enriched with the *(R)*-enantiomer.

From Fig. 10, it further appears that by operating at shorter residence times per stage, a higher overall ee_{org} is obtained at the cost of a lower overall yield of the *(S)*-enantiomer. Thus, a proper selection of the residence time and total number of stages is needed for obtaining the desired yield of the *(S)*-enantiomer and ee_{org}. Typically, at the operational conditions relevant to this figure, an overall yield of the *(S)*-enantiomer over 60% and an overall ee_{org} over 53% are obtained by operation at 4 s per stage in a five-stage cross flow configuration.

The second option for multi-stage operation is an overall countercurrent flow configuration. Inside each microreactor, we still have cocurrent slug flow of the two phases in equal flow rate. The fresh organic feed enters the first stage and flows continuously through the next stages. The aqueous feed enters at the last stage and flows in the opposite direction, see Fig. 11. Model II was again used successively for each stage to calculate the overall system performance, in combination with a trial and error method (i.e., the modelling started with a guess of the aqueous phase inlet concentrations at the first stage, until the modelled aqueous inlet at the last stage matched the fresh aqueous feed composition).

Fig. 12 depicts the effects of the total number of stages and the residence time on the overall ee_{org} and yield of the *(S)*-enantiomer. Again, the total number of stages was varied from 1 to 5 and the residence time per stage was taken as 4, 10, 22.6 or 45.2 s. With countercurrent flow conditions the overall yield of the *(S)*-enantiomer increases and the overall ee_{org} seems to decrease with an increase of the total number of stages (the latter is especially true if the residence time per stage or the total number of stages is kept short). Similarly, the overall yield of the *(S)*-enantiomer increases and the overall ee_{org} decreases with an increase of the residence time. Interestingly, the overall ee_{org} is higher than the equilibrium value in all 5 stages modelled only at relatively short residence time operations (e.g., $\tau = 4$ or 10 s per stage), which could be partly explained by the facts that the equilibrium value still increases with an increase of the total number of stages while the overall ee_{org} tends to decrease with an increase of the residence time per stage. Typically, an overall yield of the *(S)*-enantiomer of more than 50% and an overall ee_{org} of approximately 54% are obtained by operation at 4 s per stage in a five-stage countercurrent flow configuration. Although this extraction performance is slightly inferior to that in cross flow configuration under otherwise equivalent operation

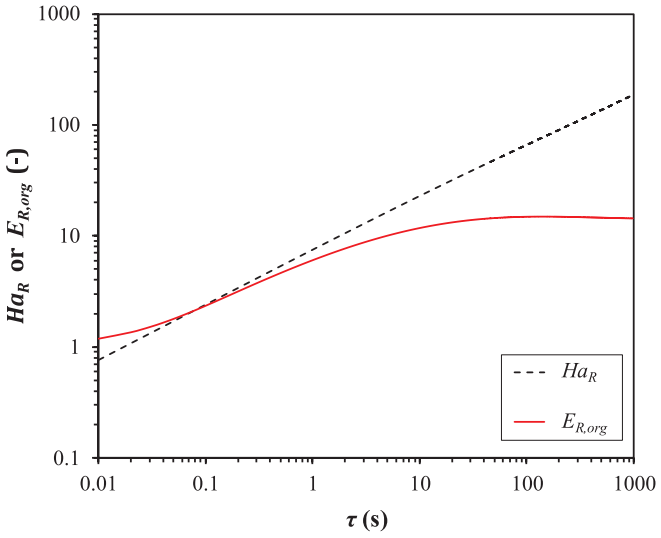

Fig. 8. Ha_R and $E_{R,org}$ as a function of the residence time according to model II.

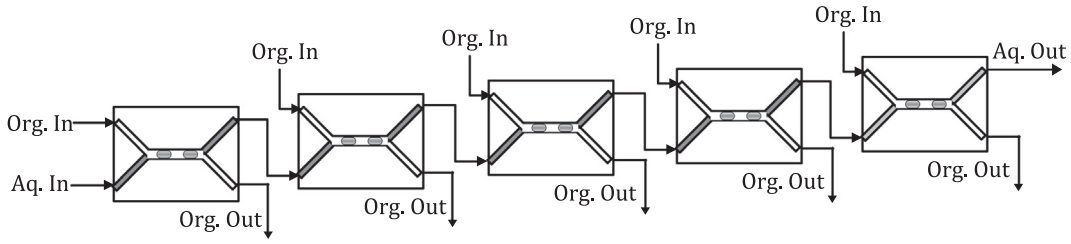

Fig. 9. Multi-stage ELLE operation in slug flow microreactors with cross flow of the organic phase. Aq. denotes the aqueous phase and Org. the organic phase.

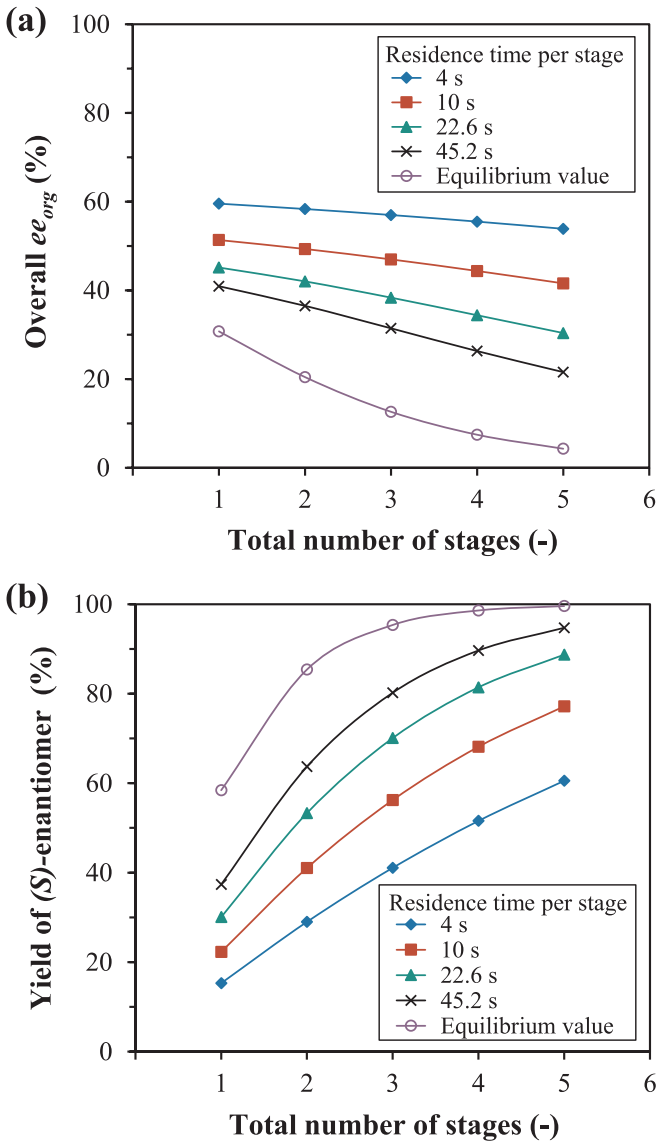

Fig. 10. Effect of the total number of stages and the residence time per stage on (a) the overall ee_{org} and (b) the overall yield of the *(S)*-enantiomer according to model II. Cross flow configuration. 1 mM host in the organic feed, 1 mM racemate in the aqueous feed. The equilibrium values are shown for comparison. Other conditions are shown in Table 1.

conditions, the countercurrent flow configuration is more attractive in terms of reduced solvent and host uses.

In Fig. 13 the single-stage operation is compared with a five-stage countercurrent operation. The total residence time is the same for the two systems. Five-stage operation provides a higher overall yield of the *(S)*-enantiomer and a higher overall ee_{org}. This effect is caused by a higher local ee_{org} in multi-stage operation due to the shorter residence time per stage. Also in the multi-stage operation larger concentration difference between the phases are found resulting in a higher amount of extraction.

The results shown in this section illustrate the usefulness of process modelling of single- and multi-stage operations. It facilitates a screening process to identify the microreactor arrangement, flow ratio of the phases and operational conditions to obtain a high overall yield and enantiomeric excess. It has to be mentioned that the modelled multi-stage operation is not optimized, given the used 1:1 aqueous to organic ratio (a pre-requisite for the validity of the overall physical or chemical mass transfer coefficient equations; cf. Eqs. (23) and (24)) [67]. To obtain a favorable *ee* of each enantiomer (e.g., close to 100%) in practical operations, the cross flow configuration might use a different aqueous-organic flow ratio per stage, and the countercurrent flow configuration might prefer to feed the aqueous racemic solution at the middle stage together with the wash water and organic feed added at the opposite ends of the stages [54]. In this respect, model II still needs to be improved with the inclusion of a more general mass transfer correlation valid for various aqueous-to-organic flow ratios, which requires additional mass transfer study in slug flow microreactors and is under our ongoing work.

5. Conclusions

This work presents a modelling study of the enantioselective extraction of an aqueous racemic 3,5-dinitrobenzoyl-*(R,S)*-leucine (1 mM) with cinchona alkaloid as the chiral host (1 mM) in 1-octanol in capillary microreactors (with an internal diameter of 0.8 mm) under slug flow operation at an aqueous to organic flow ratio of 1:1. A good agreement between the model predictions and results of extraction experiments (in terms of the exit enantiomer concentrations and enantiomeric excess) was obtained, by combining in the model the physical mass transfer rate of each enantiomer with the enhancement factor expressions that account for the aqueous dissociation of each enantiomer and its complexation with the host in the organic phase. An enantiomeric excess of the *(S)*-enantiomer higher than the equilibrium value was observed experimentally at shorter residence times in microreactors, which could be explained by an instantaneous rate of the complexation of the *(S)*-enantiomer with the host and a finite rate of the complexation of the *(R)*-enantiomer. In the model, an optimized second-order forward reaction rate constant at around 5×10^5 L/(mol·s) was found for the complexation of the *(R)*-enantiomer and has to be verified in future kinetic studies.

The model developed in this work can be used for the prediction of the enantioselective extraction performance in single- and multi-stage operations under slug flow in capillary microreactors. Thus, the model allows a pre-screening for the identification of the relevant operational conditions and multi-stage operation scheme towards obtaining high overall yield and *ee* of the enantiomer, as demonstrated in the illustration examples dealing with cross flow and countercurrent flow configurations up to five stages. However, the current model still needs to be improved in order to expand its validity for other conditions (e.g., for the aqueous-to-organic flow ratios other than 1:1 and other microreactor geometries). This is particularly relevant for performance

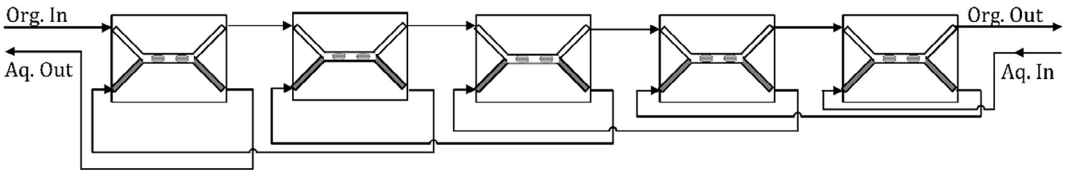

Fig. 11. Multi-stage ELLE in slug flow microreactors with an overall countercurrent flow configuration.

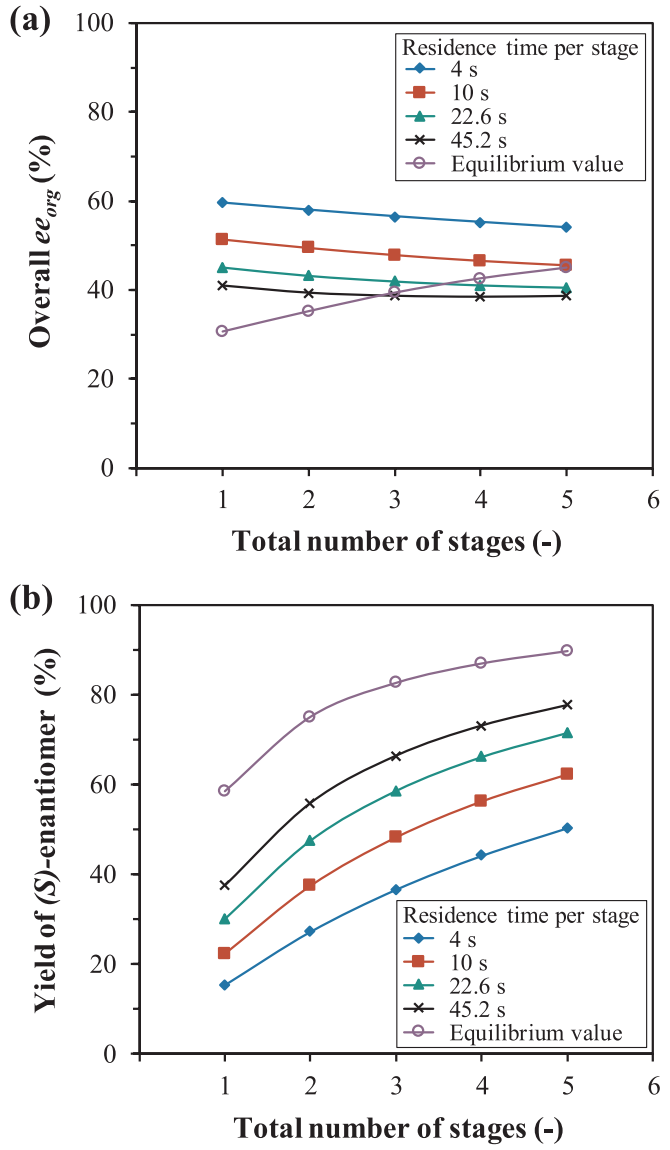

Fig. 12. Effect of the total number of stages and the residence time per stage on (a) the overall ee_{org} and (b) the overall yield of the *(S)*-enantiomer according to model II. Countercurrent flow configuration. 1 mM host in the organic feed, 1 mM racemate in the aqueous feed. The equilibrium values are shown for comparison. Other conditions are shown in Table 1.

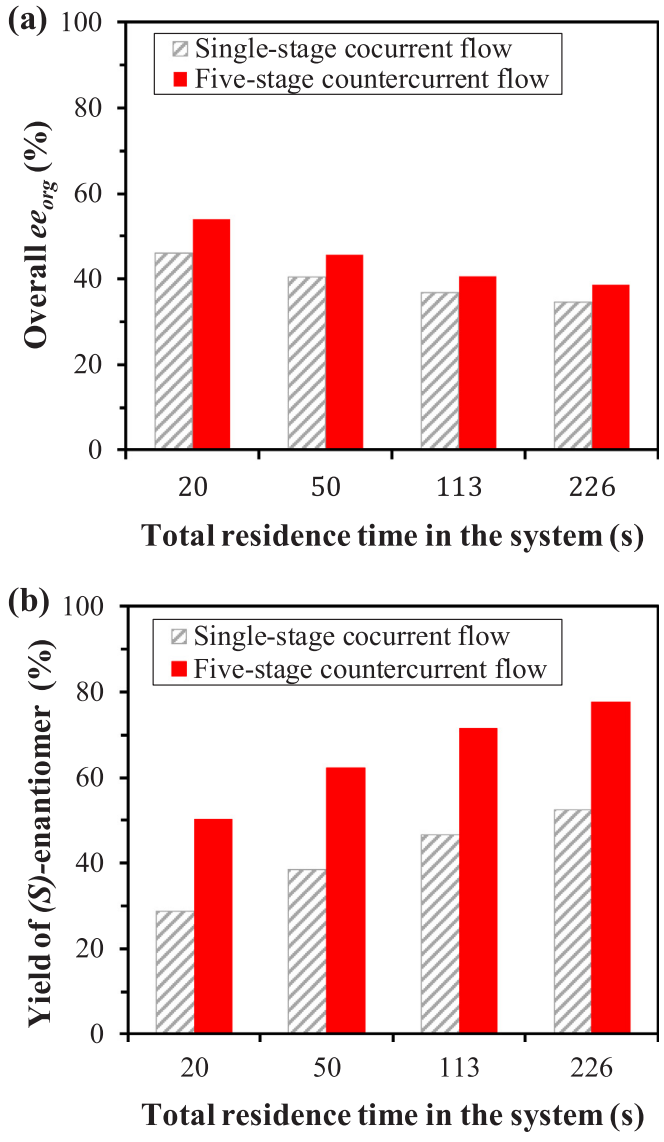

Fig. 13. (a) The overall ee_{org} and (b) the overall yield of the *(S)*-enantiomer with single-stage cocurrent flow and five-stage countercurrent flow operations according to model II. The total residence time in the system is kept the same.

predictions when using countercurrent multi-stage setups including washing, feeding and stripping sections with the objective to separate racemates in both enantiomers in high yields [54].

Acknowledgements

This work was supported by the STW (through Project 11404: Chiral Separations by Kinetic Extractive Resolution in Microfluidic Devices). Input from all user committee members of the project are gratefully acknowledged.

Appendix A. . Extraction performance as a function of the residence time

ELLE experiments in microreactors were conducted at a constant temperature of ca. 23 °C. The extraction performance (e.g., characterized by the enantiomer concentration in the aqueous phase at the microreactor outlet) was found just a function of the residence time (i.e., independent of the

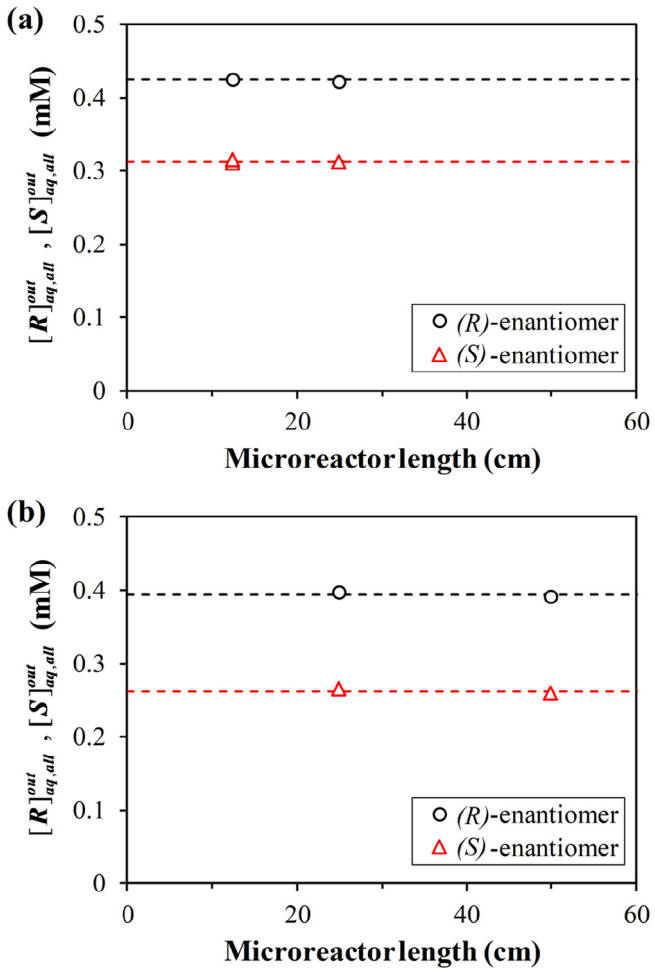

Fig. A.1. Aqueous phase exit concentrations at residence times of 45 s (a) and 90 s (b) measured in the microreactor. Residence time was kept constant by varying the capillary microreactor length and the flow rate according to Eq. (1). Dash lines are shown for visual guidance. Experimental conditions are shown in Table 1.

flow rate or microreactor length). Fig. A.1 shows the aqueous phase exit concentration of each enantiomer (in both neutral and dissociated forms) for given residence times at 45 and 90 s. A consistent exit enantiomer concentration was observed, regardless of the microreactor length in use.

Appendix B. . Enhancement factor in the aqueous phase in the presence of dissociation reaction

For a given axial location along the microreactor, the dissociation reaction of each enantiomer in the aqueous phase is assumed to be very fast (i.e., the reaction rate is instantaneous as compared with the physical transport rate of each enantiomer), so that the equilibrium was approached at all points therein. Then, according to the film theory, the total mass balance of the *(S)*-enantiomer in the film region of the aqueous side (Fig. B.1) is given by [74]

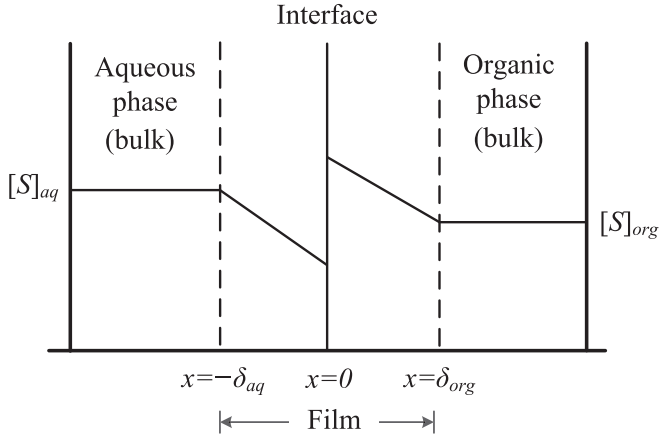

Fig. B.1. Concentration profile of the *(S)*-enantiomer in the neutral form according to the film theory for a given axial location along the microreactor.

$$D_{S,aq}\frac{d^2[S]_{aq}}{dx^2} + D_{S^-,aq}\frac{d^2[S^-]_{aq}}{dx^2} = 0 \tag{B.1}$$

Under the assumption that $D_{S,aq} \approx D_{S^-,aq}$, a general solution to the above differential equation is found as

$$[S]_{aq} + [S^-]_{aq} = f_1 x + f_2 \tag{B.2}$$

where f_1 and f_2 are constants.

The boundary conditions are

$$x = -\delta_{aq},\ [S]_{aq} = [S]_{aq,bulk}$$
$$x = 0,\ [S]_{aq} = [S]_{aq,I} \tag{B.3}$$

where $[S]_{aq,bulk}$ and $[S]_{aq,I}$ represent the concentration of the *(S)*-enantiomer (in the neutral form) in the bulk and at the interface of the aqueous side, respectively.

Since the dissociation reaction was at equilibrium at all points, there is

$$K_a = \frac{\gamma_{H^+}\gamma_{S^-}}{\gamma_S}\frac{[H^+]_{aq}[S^-]_{aq}}{[S]_{aq}} \tag{B.4}$$

Here due to the use of a buffer system (pH = 6.58), the concentration of H^+ throughout the film region and the bulk region in the aqueous phase is assume to be constant.

The molar flux of the *(S)*-enantiomer from the aqueous phase to the interface in the presence of its dissociation reaction ($J_{S,aq,chem}$) is derived as

$$J_{S,aq,chem} = -D_{S,aq}\frac{d[S]_{aq}}{dx} - D_{S^-,aq}\frac{d[S^-]_{aq}}{dx} = -f_1 \tag{B.5}$$

Finally, it is obtained upon solving Eqs. (B.2)–(B.5) that

$$J_{S,aq,chem} = \frac{\left(D_{S,aq} + \frac{D_{S^-,aq}\gamma_S K_a}{\gamma_{H^+}\gamma_{S^-}[H^+]}\right)([S]_{aq,bulk} - [S]_{aq,I})}{\delta_{aq}} \tag{B.6}$$

The molar flux of the *(S)*-enantiomer from the aqueous phase to the interface in the absence of the dissociation reaction ($J_{S,aq,phys}$) is

$$J_{S,aq,phys} = \frac{D_{S,aq}([S]_{aq,bulk} - [S]_{aq,I})}{\delta_{aq}} \tag{B.7}$$

Then, the enhancement factor to account for the presence of this dissociation reaction is

$$E_{S,aq} = \frac{J_{S,aq,chem}}{J_{S,aq,phys}} = 1 + \frac{D_{S^-,aq}\gamma_S K_a}{D_{S,aq}\gamma_{H^+}\gamma_{S^-}[H^+]_{aq}} \tag{B.8}$$

For the *(R)*-enantiomer, it is similarly obtained that

$$E_{R,aq} = 1 + \frac{D_{R^-,aq}\gamma_R K_a}{D_{R,aq}\gamma_{H^+}\gamma_{R^-}[H^+]_{aq}} \tag{B.9}$$

Under the present experimental conditions (i.e., constant H^+ concentration, the same diffusion/activity coefficient for the neutral or dissociated form of each enantiomer), $E_{S,aq}$ and $E_{R,aq}$ are equal. Thus, it is simplified that $E_{S,aq} = E_{R,aq} = E_{aq,\infty}$.

Appendix C. . Number of segments along the microreactor and its effect on the model convergence

In the modelling, the microreactor was divided axially into n equally-spaced segments. If n is sufficiently large, the extracted amount of each enantiomer into the organic phase in one segment k (k = 1, 2, …, n) is negligibly small compared with its total amount present in the aqueous phase at the inlet of this segment. Then, the concentrations of the *(S)*- and *(R)*-enantiomers in each phase, and the concentration of host in the organic phase can be assumed constant throughout each segment k during the respective modelling step. Before the modelling proceeded to the next segment

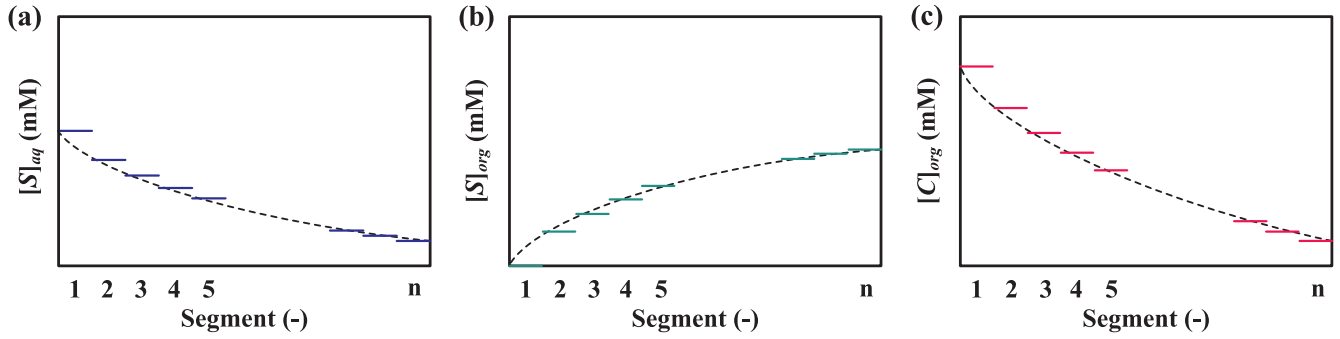

Fig. C.1. Illustration of the axial concentration profiles in the microreactor for the *(S)*-enantiomer in the aqueous phase (a) and organic phase (b), and the concentration profile of the host in the organic phase (c). The dash line represents the actual concentration profile and the solid line shown in each segment represents the modelled one.

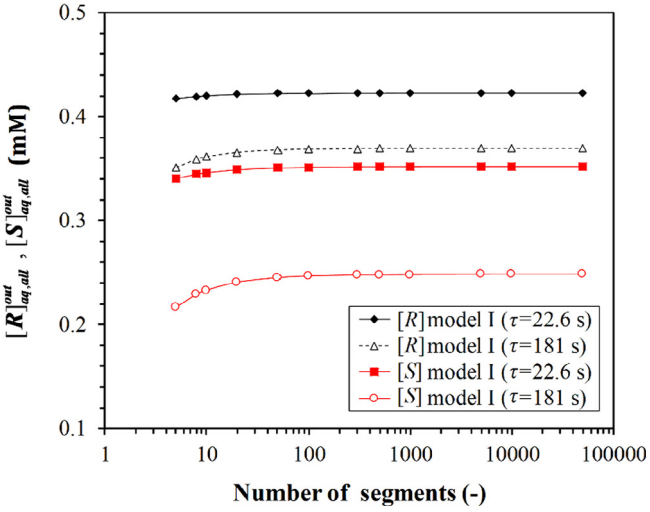

Fig. C.2. Modelled aqueous phase exit concentrations as a function of the total number of segments employed in the modelling for two representative residence time values. The complexation of each enantiomer with the host was assumed in the instantaneous reaction regime (i.e., according to model I). Other conditions are shown in Table 1.

$k+1$, the concentration values at the outlet of the segment k (equal to the corresponding ones at the inlet of the next segment) should be updated according to the extracted amount, in order to satisfy the mass balance. It is easily understood that if n value is large enough, the modelled concentration profile approaches the actual one (as illustrated in Fig. C.1).

The value of n should be also selected that the model solution convergence has been achieved. Fig. C.2 depicts the modelled concentration of each enantiomer (in both neutral and dissociated forms) in the aqueous phase exit as a function of n value under two representative residence time values. The modelled concentration quickly converges to a constant value (i.e., the correct solution) upon increasing n much above 100 for all residence time values relevant to our experiments. Thus, a sufficiently large value of n ($>$ 10,000) was used in the modelling for a comparison with the experimental measurements. Despite the large number of segments in use, the model is still efficient since the calculation time to solve the model was relatively short (on the order of minutes).

It should be noted that the modelling can be also performed using the state-of-the-art ordinary different equation (ODE) solvers in Matlab, which might be more efficient in terms of reduced number of steps and thus more appropriate for more demanding calculations such as countercurrent ELLE in microreactors involving a large number of stages.

References

[1] G. Gübitz, M.G. Schmid, Chiral separation by chromatographic and electromigration techniques. A Review, Biopharm. Drug Dispos. 22 (2001) 291–336, https://doi.org/10.1002/bdd.279.

[2] N. Grobuschek, M.G. Schmid, J. Koidl, G. Gübitz, Enantioseparation of amino acids and drugs by CEC, pressure supported CEC, and micro-HPLC using a teicoplanin aglycone stationary phase, J. Sep. Sci. 25 (2002) 1297–1302, https://doi.org/10.1002/1615-9314(20021101)25:15/17<1297::AID-JSSC1297>3.0.CO;2-X.

[3] B. Tan, G. Luo, X. Qi, J. Wang, Enantioselective extraction of d, l-tryptophan by a new chiral selector: complex formation with di(2-ethylhexyl)phosphoric acid and O, O′-dibenzoyl-(2R,3R)-tartaric acid, Sep. Purif. Technol. 49 (2006) 186–191, https://doi.org/10.1016/j.seppur.2005.09.010.

[4] W.H.D. Camp, The FDA perspective on the development of stereoisomers, Chirality 1 (1989) 2–6, https://doi.org/10.1002/chir.530010103.

[5] A.M. Rouhi, Chiral business, Chem. Eng. News Arch. 81 (2003) 45–61, https://doi.org/10.1021/cen-v081n018.p045.

[6] M. Steensma, N.J.M. Kuipers, A.B. De Haan, G. Kwant, Identification of enantioselective extractants for chiral separation of amines and aminoalcohols, Chirality 18 (2006) 314–328, https://doi.org/10.1002/chir.20258.

[7] T. Yutthalekha, C. Wattanakit, V. Lapeyre, S. Nokbin, C. Warakulwit, J. Limtrakul, A. Kuhn, Asymmetric synthesis using chiral-encoded metal, Nat. Commun. 7 (2016) 12678, https://doi.org/10.1038/ncomms12678.

[8] H. Lorenz, A. Seidel-Morgenstern, Processes to separate enantiomers, Angew. Chem. Int. Ed. 53 (2014) 1218–1250, https://doi.org/10.1002/anie.201302823.

[9] F. Faigl, E. Fogassy, M. Nógrádi, E. Pálovics, J. Schindler, Strategies in optical resolution: a practical guide, Tetrahedron: Asymmetry. 19 (2008) 519–536, https://doi.org/10.1016/j.tetasy.2008.02.004.

[10] E. Fogassy, M. Nógrádi, D. Kozma, G. Egri, E. Pálovics, V. Kiss, Optical resolution methods, Org. Biomol. Chem. 4 (2006) 3011–3030, https://doi.org/10.1039/B603058K.

[11] M. Leeman, G. Brasile, E. Gelens, T. Vries, B. Kaptein, R. Kellogg, Structural aspects of nucleation inhibitors for diastereomeric resolutions and the relationship to Dutch resolution, Angew. Chem. Int. Ed. 47 (2008) 1287–1290, https://doi.org/10.1002/anie.200704021.

[12] H. Lorenz, F. Czapla, D. Polenske, M.P. Elsner, A. Seidel-Morgenstern, Crystallization based separation of enantiomers (Review), J. Univ. Chem. Technol. Metall. 42 (2007) 5–16, https://doi.org/10.17617/2.1757057.

[13] A. De Haan, B. Simandi, Extraction technology for the separation of optical isomers, in: J.A. Marcus, Yizhak SenGupta, Arup K. Marinsky (Eds.), Ion Exch. Solvent Extr. Ser. Adv. Marcel Dekker Inc., New York, 2001.

[14] N.M. Maier, P. Franco, W. Lindner, Separation of enantiomers: needs, challenges, perspectives, J. Chromatogr. A 906 (2001) 3–33, https://doi.org/10.1016/S0021-9673(00)00532-X.

[15] T.J. Ward, K.D. Ward, Chiral separations: Fundamental review 2010, Anal. Chem. 82 (2010) 4712–4722, https://doi.org/10.1021/ac1010926.

[16] A. Rajendran, G. Paredes, M. Mazzotti, Simulated moving bed chromatography for the separation of enantiomers, J. Chromatogr. A. 1216 (2009) 709–738, https://doi.org/10.1016/j.chroma.2008.10.075.

[17] J.T.F. Keurentjes, L.J.W.M. Nabuurs, E.A. Vegter, Liquid membrane technology for the separation of racemic mixtures, J. Membr. Sci. 113 (1996) 351–360, https://doi.org/10.1016/0376-7388(95)00176-X.

[18] R. Xie, L.-Y. Chu, J.-G. Deng, Membranes and membrane processes for chiral resolution, Chem. Soc. Rev. 37 (2008) 1243–1263, https://doi.org/10.1039/B713350B.

[19] R. Molinari, P. Argurio, Supported liquid membrane stability in chiral resolution by chemically and physically modified membranes, Ann. Chim. 91 (2001) 191–196.

[20] B. Baragaña, A.G. Blackburn, P. Breccia, A.P. Davis, J. de Mendoza, J.M. Padrón-Carrillo, P. Prados, J. Riedner, J.G. de Vries, Enantioselective transport by a steroidal guanidinium receptor, Chem. Eur. J. 8 (2002) 2931–2936, https://doi.org/10.1002/1521-3765(20020703)8:13<2931::AID-CHEM2931>3.0.CO;2-H.

[21] A. Gössi, W. Riedl, B. Schuur, Enantioseparation with liquid membranes, J. Chem. Technol. Biotechnol. 93 (2017) 629–644, https://doi.org/10.1002/jctb.5417.

[22] X. Chen, J. Wang, F. Jiao, Efficient enantioseparation of phenylsuccinic acid enantiomers by aqueous two-phase system-based biphasic recognition chiral extraction: phase behaviors and distribution experiments, Process Biochem. 50 (2015) 1468–1478, https://doi.org/10.1016/j.procbio.2015.05.014.

[23] M. Choi, M.-J. Jun, K.M. Kim, Efficient synthesis of chiral binaphthol aldehyde with phenyl ether linkage for enantioselective extraction of amino acids, Bull. Korean Chem. Soc. 36 (2015) 1834–1837, https://doi.org/10.1002/bkcs.10354.

[24] S. Corderí, C.R. Vitasari, M. Gramblicka, T. Giard, B. Schuur, Chiral separation of naproxen with immobilized liquid phases, Org. Process Res. Dev. 20 (2016) 297–305, https://doi.org/10.1021/acs.oprd.6b00020.

[25] A. Holbach, J. Godde, R. Mahendrarajah, N. Kockmann, Enantioseparation of chiral aromatic acids in process intensified liquid–liquid extraction columns, AIChE J. 61

(2015) 266–276, https://doi.org/10.1002/aic.14654.
[26] A. Holbach, S. Soboll, B. Schuur, N. Kockmann, Chiral separation of 3,5-dinitrobenzoyl-(R, S)-leucine in process intensified extraction columns, Ind. Eng. Chem. Res. 54 (2015) 8266–8276, https://doi.org/10.1021/acs.iecr.5b00896.
[27] H. Huang, Q. Chen, M. Choi, R. Nandhakumar, Z. Su, S. Ham, K.M. Kim, Highly enantioselective extraction of underivatized amino acids by the uryl-pendant hydroxyphenyl-binol ketone, Chem. Eur. J. 20 (2014) 2895–2900, https://doi.org/10.1002/chem.201304454.
[28] H. Huang, R. Nandhakumar, M. Choi, Z. Su, K.M. Kim, Enantioselective liquid–liquid extractions of underivatized general amino acids with a chiral ketone extractant, J. Am. Chem. Soc. 135 (2013) 2653–2658, https://doi.org/10.1021/ja3105945.
[29] J. Koska, D.Y.C. Choy, P. Francis, A.L. Creagh, C.A. Haynes, Thermodynamic modeling of multi-staged extraction systems for chiral separations through coupled analysis of species equilibria and mass transfer, Sep. Sci. Technol. 49 (2014) 635–646, https://doi.org/10.1080/01496395.2013.868489.
[30] Y. Peng, Q. He, B. Zuo, H. Niu, T. Tong, H. Zhao, Enantioselective liquid–liquid extraction of zopiclone with mandelic acid ester derivatives, Chirality 25 (2013) 952–956, https://doi.org/10.1002/chir.22239.
[31] T.P. Quinn, P.D. Atwood, J.M. Tanski, T.F. Moore, J.F. Folmer-Andersen, Aza-crown macrocycles as chiral solvating agents for mandelic acid derivatives, J. Org. Chem. 76 (2011) 10020, https://doi.org/10.1021/jo2018203.
[32] B. Schuur, J. Floure, A.J. Hallett, J.G.M. Winkelman, J.G. de Vries, H.J. Heeres, Continuous chiral separation of amino acid derivatives by enantioselective liquid − liquid extraction in centrifugal contactor separators, Org. Process Res. Dev. 12 (2008) 950–955, https://doi.org/10.1021/op800074w.
[33] B. Schuur, A.J. Hallett, J.G.M. Winkelman, J.G. de Vries, H.J. Heeres, Scalable enantioseparation of amino acid derivatives using continuous liquid − liquid extraction in a cascade of centrifugal contactor separators, Org. Process Res. Dev. 13 (2009) 911–914, https://doi.org/10.1021/op900152e.
[34] B.J.V. Verkuijl, B. Schuur, A.J. Minnaard, J.G. de Vries, B.L. Feringa, Chiral separation of substituted phenylalanine analogues using chiral palladium phosphine complexes with enantioselective liquid–liquid extraction, Org. Biomol. Chem. 8 (2010) 3045–3054, https://doi.org/10.1039/B924749A.
[35] B. Schuur, B.J.V. Verkuijl, A.J. Minnaard, J.G. de Vries, H.J. Heeres, B.L. Feringa, Chiral separation by enantioselective liquid–liquid extraction, Org. Biomol. Chem. 9 (2010) 36–51, https://doi.org/10.1039/C0OB00610F.
[36] B. Schuur, B.J.V. Verkuijl, J. Bokhove, A.J. Minnaard, J.G. de Vries, H.J. Heeres, B.L. Feringa, Enantioselective liquid–liquid extraction of (R, S)-phenylglycinol using a bisnaphthyl phosphoric acid derivative as chiral extractant, Tetrahedron. 67 (2011) 462–470, https://doi.org/10.1016/j.tet.2010.11.001.
[37] M. Steensma, N.J. Kuipers, A.B. de Haan, G. Kwant, Influence of process parameters on extraction equilibria for the chiral separation of amines and amino-alcohols with a chiral crown ether, J. Chem. Technol. Biotechnol. 81 (2006) 588–597, https://doi.org/10.1002/jctb.1434.
[38] M. Steensma, N.J.M. Kuipers, A.B. de Haan, G. Kwant, Modelling and experimental evaluation of reaction kinetics in reactive extraction for chiral separation of amines, amino acids and amino-alcohols, Chem. Eng. Sci. 62 (2007) 1395–1407, https://doi.org/10.1016/j.ces.2006.11.043.
[39] N. Sunsandee, U. Pancharoen, P. Rashatasakhon, P. Ramakul, N. Leepipatpiboon, Enantioselective separation of racemic amlodipine by two-phase chiral extraction containing O, O′-dibenzoyl-(2S,3S)-tartaric acid as chiral selector, Sep. Sci. Technol. 48 (2013) 2363–2371, https://doi.org/10.1080/01496395.2013.804088.
[40] N. Sunsandee, N. Leepipatpiboon, P. Ramakul, T. Wongsawa, U. Pancharoen, The effects of thermodynamics on mass transfer and enantioseparation of (R, S)-amlodipine across a hollow fiber supported liquid membrane, Sep. Purif. Technol. 102 (2013) 50–61, https://doi.org/10.1016/j.seppur.2012.09.027.
[41] K. Tang, T. Fu, P. Zhang, Enantioselective liquid–liquid extraction of (D, L)-valine using metal–BINAP complex as chiral extractant, J. Chem. Technol. Biotechnol. 88 (2013) 1920–1929, https://doi.org/10.1002/jctb.4051.
[42] J. Wang, H. Yang, J. Yu, X. Chen, F. Jiao, Macrocyclic β-cyclodextrin derivative-based aqueous-two phase systems: Phase behaviors and applications in enantioseparation, Chem. Eng. Sci. 143 (2016) 1–11, https://doi.org/10.1016/j.ces.2015.12.019.
[43] B. Schuur, M. Steensma, J.G.M. Winkelman, J.G. de Vries, de A.B. Haan, H.J. Heeres, Continuous enantioseparation by liquid-liquid extraction, Chim. Oggi 27 (2009) 9–12.
[44] S. Susanti, T.G. Meinds, E.B. Pinxterhuis, B. Schuur, J.G. de Vries, B.L. Feringa, J.G.M. Winkelman, J. Yue, H.J. Heeres, Proof of concept for continuous enantioselective liquid–liquid extraction in capillary microreactors using 1-octanol as a sustainable solvent, Green Chem. 19 (2017) 4334–4343, https://doi.org/10.1039/C7GC01700F.
[45] V. Zgonnik, S. Gonella, M.-R. Mazières, F. Guillen, G. Coquerel, N. Saffon, J.-C. Plaquevent, Design and scalable synthesis of new chiral selectors. Part 2: chiral ionic liquids derived from diaminocyclohexane and histidine, Org. Process Res. Dev. 16 (2012) 277–285, https://doi.org/10.1021/op200082a.
[46] K. Tang, H. Zhang, Y. Liu, Experimental and simulation on enantioselective extraction in centrifugal contactor separators, AIChE J. 59 (2013) 2594–2602, https://doi.org/10.1002/aic.14004.
[47] K. Tang, X. Feng, P. Zhang, S. Yin, C. Zhou, C. Yang, Experimental and model study on multistage enantioselective liquid–liquid extraction of ketoconazole enantiomers in centrifugal contactor separators, Ind. Eng. Chem. Res. 54 (2015) 8762–8771, https://doi.org/10.1021/acs.iecr.5b01722.
[48] K. Tang, H. Zhang, P. Zhang, Continuous separation of α-cyclohexyl-mandelic acid enantiomers by enantioselective liquid–liquid extraction in centrifugal contactor separators: experiments and modeling, Ind. Eng. Chem. Res. 52 (2013) 3893–3902, https://doi.org/10.1021/ie303291a.
[49] P. Zhang, S. Wang, K. Tang, W. Xu, F. He, Y. Qiu, Modeling multiple chemical equilibrium in chiral extraction of metoprolol enantiomers from single-stage extraction to fractional extraction, Chem. Eng. Sci. 177 (2018) 74–88, https://doi.org/10.1016/j.ces.2017.11.007.
[50] R.M.C. Viegas, C.A.M. Afonso, J.G. Crespo, I.M. Coelhoso, Modelling of the enantioselective extraction of propranolol in a biphasic system, Sep. Purif. Technol. 53 (2007) 224–234, https://doi.org/10.1016/j.seppur.2006.07.010.
[51] J. Koska, C.A. Haynes, Modelling multiple chemical equilbria in chiral partition systems, Chem. Eng. Sci. 56 (2001) 5853–5864, https://doi.org/10.1016/S0009-2509(00)00419-X.
[52] S.K. Tulashie, H. Kaemmerer, H. Lorenz, A. Seidel-Morgenstern, Solid − liquid equilibria of mandelic acid enantiomers in two chiral solvents: experimental determination and model correlation, J. Chem. Eng. Data 2010 (55) (2009) 333–340, https://doi.org/10.1021/je900353b.
[53] M. Saric, L.A.M. van der Wielen, A.J.J. Straathof, Theoretical performance of countercurrent reactors for production of enantiopure compounds, Chem. Eng. Sci. 66 (2011) 510–518, https://doi.org/10.1016/j.ces.2010.11.020.
[54] B. Schuur, J.G.M. Winkelman, J.G. de Vries, H.J. Heeres, Experimental and modeling studies on the enantio-separation of 3,5-dinitrobenzoyl-(R),(S)-leucine by continuous liquid–liquid extraction in a cascade of centrifugal contactor separators, Chem. Eng. Sci. 65 (2010) 4682–4690, https://doi.org/10.1016/j.ces.2010.05.015.
[55] M.N. Kashid, Y.M. Harshe, D.W. Agar, Liquid − liquid slug flow in a capillary: an alternative to suspended drop or film contactors, Ind. Eng. Chem. Res. 46 (2007) 8420–8430, https://doi.org/10.1021/ie070077x.
[56] Y. Kikutani, K. Mawatari, A. Hibara, T. Kitamori, Circulation microchannel for liquid–liquid microextraction, Microchim. Acta 164 (2008) 241–247, https://doi.org/10.1007/s00604-008-0065-7.
[57] Y.S. Huh, S.J. Jeon, E.Z. Lee, H.S. Park, W.H. Hong, Microfluidic extraction using two phase laminar flow for chemical and biological applications, Korean J. Chem. Eng. 28 (2011) 633–642, https://doi.org/10.1007/s11814-010-0533-8.
[58] E. Kamio, Y. Seike, H. Yoshizawa, H. Matsuyama, T. Ono, Microfluidic extraction of docosahexaenoic acid ethyl ester: comparison between slug flow and emulsion, Ind. Eng. Chem. Res. 50 (2011) 6915–6924, https://doi.org/10.1021/ie102207c.
[59] D. Ciceri, J.M. Perera, G.W. Stevens, The use of microfluidic devices in solvent extraction, J. Chem. Technol. Biotechnol. 89 (2014) 771–786, https://doi.org/10.1002/jctb.4318.
[60] N. Assmann, A. Ładosz, P. Rudolf von Rohr, Continuous micro liquid-liquid extraction, Chem. Eng. Technol. 36 (2013) 921–936, https://doi.org/10.1002/ceat.201200557.
[61] L. Hohmann, S.K. Kurt, S. Soboll, N. Kockmann, Separation units and equipment for lab-scale process development, J. Flow Chem. 6 (2016) 181–190, https://doi.org/10.1556/1846.2016.00024.
[62] K. Wang, G. Luo, Microflow extraction: a review of recent development, Chem. Eng. Sci. 169 (2017) 18–33, https://doi.org/10.1016/j.ces.2016.10.025.
[63] A. Holbach, N. Kockmann, Counter-current arrangement of microfluidic liquid-liquid droplet flow contactors, Green Process. Synth. 2 (2013) 157–167, https://doi.org/10.1515/gps-2013-0006.
[64] E.Y. Kenig, Y. Su, A. Lautenschleger, P. Chasanis, M. Grünewald, Micro-separation of fluid systems: a state-of-the-art review, Sep. Purif. Technol. 120 (2013) 245–264, https://doi.org/10.1016/j.seppur.2013.09.028.
[65] K.S. Elvira, X.C. i Solvas, R.C.R. Wootton, A.J. deMello, The past, present and potential for microfluidic reactor technology in chemical synthesis, Nat. Chem. 5 (2013) 905–915, https://doi.org/10.1038/nchem.1753.
[66] A.J. Hallett, G.J. Kwant, J.G. de Vries, Continuous separation of racemic 3,5-dinitrobenzoyl-amino acids in a centrifugal contact separator with the aid of cinchona-based chiral host compounds, Chem. Eur. J. 15 (2009) 2111–2120, https://doi.org/10.1002/chem.200800797.
[67] S. Susanti, J.G.M. Winkelman, B. Schuur, H.J. Heeres, J. Yue, Lactic acid extraction and mass transfer characteristics in slug flow capillary microreactors, Ind. Eng. Chem. Res. 55 (2016), https://doi.org/10.1021/acs.iecr.5b04917.
[68] D. Jaritsch, A. Holbach, N. Kockmann, Counter-current extraction in microchannel flow: current status and perspectives, J. Fluids Eng. 136 (2014) 091211 091211 10.1115/1.4026608.
[69] W. Lindner, M. Laemmerhofer, N. Maier, Cinchonan based chiral selectors for separation of stereoisomers, US6313247B1, 2001. https://patents.google.com/patent/US6313247B1/en.
[70] B. Schuur, J.G.M. Winkelman, H.J. Heeres, Equilibrium studies on enantioselective liquid − liquid amino acid extraction using a cinchona alkaloid extractant, Ind. Eng. Chem. Res. 47 (2008) 10027–10033, https://doi.org/10.1021/ie800668e.
[71] P.V. Danckwerts, Gas-liquid Reactions, McGraw-Hill, New York, 1970.
[72] M. Eigen, Proton transfer, acid-base catalysis, and enzymatic hydrolysis. Part I: elementary processes, Angew. Chem. Int. Ed. 3 (1964) 1–19, https://doi.org/10.1002/anie.196400011.
[73] K. Onda, E. Sada, T. Kobayashi, M. Fujine, Gas absorption accompanied by complex chemical reactions- I Reversible chemical reactions, Chem. Eng. Sci. 25 (1970) 753–760, https://doi.org/10.1016/0009-2509(70)85110-7.
[74] D.R. Olander, Simultaneous mass transfer and equilibrium chemical reaction, AIChE J. 6 (1960) 233–239, https://doi.org/10.1002/aic.690060214.
[75] R.A. Robinson, R.H. Stokes, R.G. Bates, Electrolyte Solutions: The Measurement and

Interpretation of Conductance, Chemical Potential and Diffusion in Solutions of Simple Electrolytes, second ed., Butterworths Scientific Publications, London, 1959.
[76] C.J. Geankoplis, Mass Transport Phenomena, Holt, Rinehart and Winston, New York, 1972.
[77] E.L. Cussler, Diffusion: Mass Transfer in Fluid Systems, Cambridge University Press, New York, 1997.
[78] D.R. Lide, CRC Handbook of Chemistry and Physics: A Ready-reference Book of Chemical and Physical Data, CRC, Boca Raton, Fla.; London, 2007.
[79] N.R. Draper, H. Smith, Applied Regression Analysis, third ed., John Willey & Sons, Canada, 1998.
[80] J. Yue, E.V. Rebrov, J.C. Schouten, Enhancement factor for gas absorption in a finite liquid layer. Part 1: instantaneous reaction in a liquid in plug flow, Chem. Eng. Technol. 35 (2012) 679–692, https://doi.org/10.1002/ceat.201100686.
[81] F. Trachsel, A. Günther, S. Khan, K.F. Jensen, Measurement of residence time distribution in microfluidic systems, Chem. Eng. Sci. 60 (2005) 5729–5737, https://doi.org/10.1016/j.ces.2005.04.039.